J Nanostruct 16(4): 5702-5714, Autumn 2026

RESEARCH PAPER

Comparative Structural and Antibacterial Investigation of $CuFe_2O_4$ Nano-Ferrites Modified with Zn- and Co ions

*Azhar Jabbar Bohan [1], Shams N. Almutalabi [1], Israa Abass Rashed [1], Aliaa Mohsen Jabbar [2], Manar Abd Alrazaq Hassan [3], Aynoor Ibrahim Ali [4], Makarim H. Abdulkareem [5], Ghaed Khalef Salman [1], Saja Mohsen Alardhi [1], Mohammed H Abd Ali [4]**

[1] *Institute of Nanotechnology and Advanced Materials Research for Graduate Studies, University of Technology, Baghdad, Iraq*

[2] *College of Dentistry, University of Baghdad, Baghdad, Iraq*

[3] *Department of Clinical Dentistry, College of Dentistry, University of Diyala, Diyala, 34001, Iraq*

[4] *Environmental Research Center, University of Technology, Baghdad, Iraq*

[5] *Metallurgy Department, College of Production and Metallurgy, University of Technology, Baghdad, Iraq*

ARTICLE INFO

Article History:
Received 12 May 2026
Accepted 19 September 2026
Published 01 October 2026

Keywords:
Antibacterial Activity
Co-Precipitation Method
Cu-Ferrite Nanoparticles
Nano Ferrite
Nano Materials

ABSTRACT

Zn^{2+} and Co^{2+} precursors were added during synthesis to create $CuFe_2O_4$-based nanoferrite materials using the co-precipitation method. Characterization of prepared ferrite nanoparticles was achieved using FTIR, XRD, and SEM devices. The FTIR result confirmed that spinel $CuFe_2O_4$ nanoparticle structures have been identified at a wave number of 567.07 cm^{-1} shifted toward lower values (560 and 561 cm^{-1}) when Co and Zn are added. Diffraction patterns mostly attributable to a cubic spinel ferrite structure were discovered by XRD analysis, with structural parameter changes seen in the samples containing Zn and Co, Particle morphologies with visible pores and different levels of aggregation of particles were observed in the SEM images. In compared to the unmodified $CuFe_2O_4$ sample, the Zn- and Co-modified samples showed discernible alterations in surface morphology, including variations in roughness of the surface and aggregation behavior. The antibacterial outcomes showed strong action against both Gram-positive Staphylococcus aureus and Gram-negative Escherichia coli. While CF-Co demonstrated similar efficacy against both bacterial strains, with slightly higher killing of S. aureus at 5 mg/mL, CF and CF-Zn generally shown higher death percentages against E. coli. Overall, the composition of the nanoferrite and the type of bacteria both affected the antibacterial response.

How to cite this article
Bohan A., Almutalabi S., Rashed I. et al. Comparative Structural and Antibacterial Investigation of $CuFe_2O_4$ Nano-Ferrites Modified with Zn- and Co ions. J Nanostruct, 2026; 16(4):5702-5714. DOI: 10.22052/JNS.2026.04.099

INTRODUCTION

Nowadays, soft ferrite nanoparticles (NPs) are widely used in various technological applications [1, 2]. Which are important inorganic nanostructures that can be used as catalytic magnetic agents due to their remarkable features [3]; their structure is based on a closed-packed oxygen lattice with 32 partially filled octahedral (B-sites) and 64 partially filled tetrahedral (A-sites) sites and classified depending on the kind of ions occupying A-sites,

* *Corresponding Author Email: mohammed.h.abdali@uotechnology.edu.iq*

This work is licensed under the Creative Commons Attribution 4.0 International License.
To view a copy of this license, visit http://creativecommons.org/licenses/by/4.0/.

and a typical spinel is produced when only divalent ions occupy A-sites. Soft ferrite NPs, like other nanomaterials, have a high surface area to volume ratio, which gives them a number of exceptional physical and chemical characteristics [4].

A polycrystalline complex structure made up of crystals, grain boundaries, and pores is known as copper-zinc-cobalt ferrite (Cu-Zn-Co ferrite) [5, 6], which is thought to be one of the most important magnetic oxides because it has great mechanical hardness, low cost, the ability to change the magnetic properties, and the capacity to function at higher frequencies—qualities better than its monometallic counterparts. It also has a comparatively high Curie temperature; therefore, mixed metal ferrites are created [7-9].

Spinel ferrites are magnetic materials of great technical significance and potential uses in various scientific applications due to their electronic and electrical and medical properties that make them important in medical applications, especially the antibacterial properties. In addition to different compositions, which can be changed according to the proportions and types of elements added to the ferrite material [10], it is known that antibacterial activity is size-dependent, and the combination of magnetic and antibacterial properties makes this material highly valuable in biomedical applications like drug delivery and antibacterial, anticancer, and antioxidant [11, 12]. This is due to each ion affecting the bacterial cell structure differently, where Cu works to disrupt the bacterial membrane and interfere with the synthesis of bacterial DNA and proteins, The structural and physicochemical characteristics of ferrite materials, as well as their interactions with bacterial cells, may be impacted by the presence of certain metal ions, such as copper, zinc, and cobalt. However, the particular contributions that each ion makes to antibacterial activity vary depending on the experimental setup and material composition. Therefore, unless there is concrete experimental proof, potential synergistic effects between certain metal ions should be regarded with caution [13]. The antibacterial efficacy of spinel-structured ferrite nanoparticles can be influenced by several factors, including their crystallite size, chemical composition, surface properties, and this effect on interactions with bacterial cells. The presence of various metal ions—such as copper, zinc, and cobalt—may contribute to variations in the physicochemical properties of ferrite materials, and their antibacterial activity. The specific antibacterial mechanisms associated with these ions—including potential ion-related effects, oxidative processes, and interactions with bacterial cell membranes—were not directly investigated in this study. Therefore, these mechanisms should be viewed as plausible explanations based on prior research, rather than as experimentally confirmed findings. It also opens a new approach to synthesizing new materials that are more effective in medical and biological applications.

Despite numerous studies on magnetic materials and their importance, the focus on their biological applications and doping with other elements has been limited; therefore, this research aims primarily at the fabrication of magnetic Nano materials doped with safe and non-toxic elements possessing both magnetic and antibacterial properties that can be used in biomedical, environmental, and pharmaceutical applications, as well as in the broader health and hygiene sectors, making them a foundation for the development of next-generation drugs.

MATERIALS AND METHODS

Materials

Iron (III) chloride ($FeCl_3$, ≥99%), copper (II) chloride ($CuCl_2$, ≥99%), zinc chloride ($ZnCl_2$, ≥98%), cobalt (II) chloride ($CoCl_2$, ≥98%), and sodium hydroxide (NaOH, ≥98%) were purchased from Sigma-Aldrich (USA) and used as received without further purification. Distilled water was used throughout all synthesis procedures.

Preparation of Nano ferrite

The nanoferrites ($CuFe_2O_4$(CF), Zn-modified $CuFe_2O_4$(CF-Zn), and Co-modified $CuFe_2O_4$(CF-Co)) were synthesized using the co-precipitation method [14, 15].

For the preparation of $CuFe_2O_4$, $FeCl_3$ (0.1 M) and $CuCl_2$ (0.05 M) were separately dissolved in distilled water (150 ml for each solution). The two solutions were then mixed together under continuous magnetic stirring to obtain a homogeneous solution.

To prepare samples containing zinc (Zn) and cobalt (Co), 150 mL of either a zinc chloride ($ZnCl_2$, 0.05 M) or cobalt chloride ($CoCl_2$, 0.05 M) solution—added separately—was introduced into a mixture consisting of iron(III) chloride ($FeCl_3$, 0.1 M) and copper(II) chloride ($CuCl_2$, 0.05 M). Based on the concentrations and volumes of the

CC BY

starting materials, the nominal molar ratios of the elements (Fe:Cu:Zn or Fe:Cu:Co) were 2:1:1 in both cases. The zinc (Zn^{2+}) or cobalt (Co^{2+}) ions were incorporated during the co-precipitation process to investigate their influence on the structural properties and antibacterial activity of the resulting ferrite-based materials.

Sodium hydroxide solution was prepared by dissolving (3.9 g) of NaOH in 100 ml of distilled water. The NaOH solution was added dropwise to the mixed metal salt solution while stirring until the pH reached 10. At this pH value, ferrite precipitation occurred, resulting in the formation of the ferrite precursor.

The obtained precipitate was separated and washed several times with distilled water to remove residual impurities and chloride ions. The washed precipitate was then dried at 60°C and subsequently annealed at 800°C for 3h to obtain the final crystalline ferrite nanoparticles. The complete synthesis procedure is illustrated in Fig. 1.

It should be noted that the stated molar ratios represent the proportions of the starting materials added initially and do not necessarily reflect the final chemical composition of the synthesized materials as determined experimentally. Given that no elemental composition analysis (such as EDS or ICP) was performed, it is not possible to definitively ascertain how the zinc (Zn^{2+}) and cobalt (Co^{2+}) ions are incorporated into the crystal lattice of the spinel-structured copper ferrite ($CuFe_2O_4$), nor to identify the specific crystallographic sites occupied by these ions. Consequently, the discussion regarding the zinc- and cobalt-containing samples focuses on the modifications introduced via the starting materials and the observed structural changes, rather than classifying them as definitively confirmed substitutional solid solutions.

Characterization

X-ray diffraction (XRD) analysis was performed using an XRD-6000 diffractometer (Shimadzu,

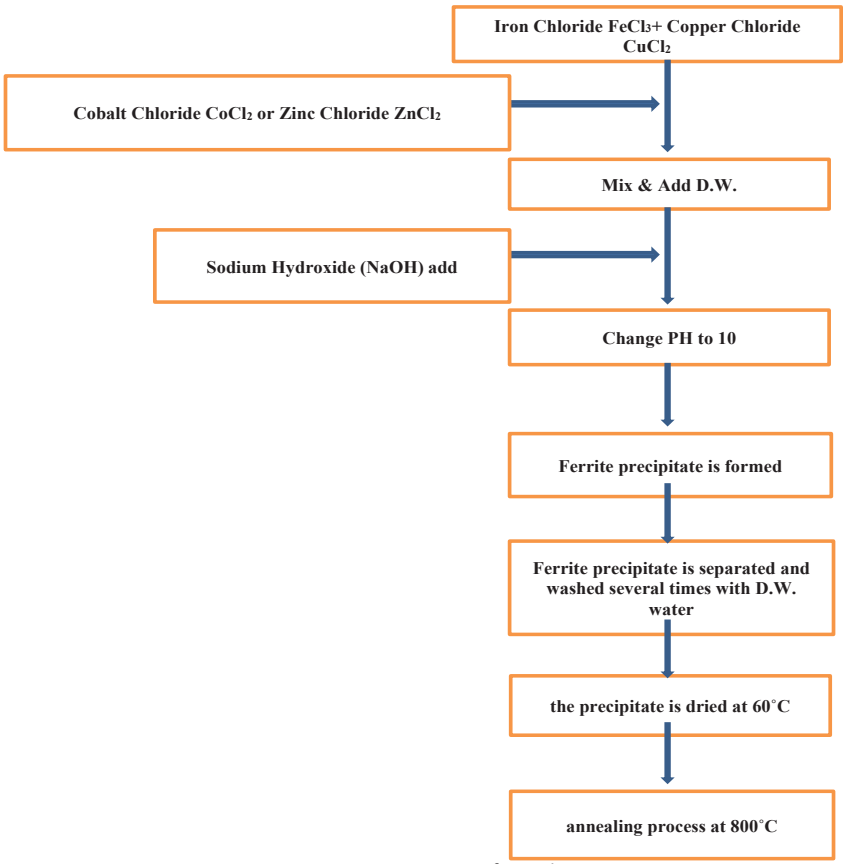


Fig. 1. Preparation steps of samples.

CC BY

Japan) with Cu Kα radiation (λ = 0.15405 nm). The instrument was operated at 60 kV and 80 mA, and diffraction patterns were collected over a 2θ range of 10–80° at a scan rate of 6° min^{-1}. The morphology of the synthesized nanoferrites ($CuFe_2O_4$(CF), Zn-modified $CuFe_2O_4$(CF-Zn), and Co-modified $CuFe_2O_4$(CF-Co)) was characterized using a VEGA 3 SB scanning electron microscope (Tescan, Czech Republic) operated at an accelerating voltage of 20 kV. Attenuated Total Reflection–Fourier Transform Infrared (ATR–FTIR) spectra were recorded using a Bruker ALPHA II spectrometer (Germany) in the range of 4000–400 cm^{-1} to identify the functional groups present in the synthesized materials.

Materials and Methods of Antibacterial Tests

Three concentrations (1.25, 2.5, and 5 mg/ml) of pure nanoferrite materials and modified ones ($CuFe_2O_4$(CF), Zn-modified $CuFe_2O_4$(CF-Zn), and Co-modified $CuFe_2O_4$(CF-Co)) were used to test against two types of bacteria, E. coli (gram-negative bacteria) and Staphylococcus aureus (gram-positive bacteria), by dilution methods according to [5] in the University of Technology (Nanotechnology and Advanced Materials Research Center). After activating the bacteria in nutrient agar at 37°C for 24 h, it's mixed with these materials at a concentration of 10^7 cfu/ml and incubated in a shaking incubator at 37°C for

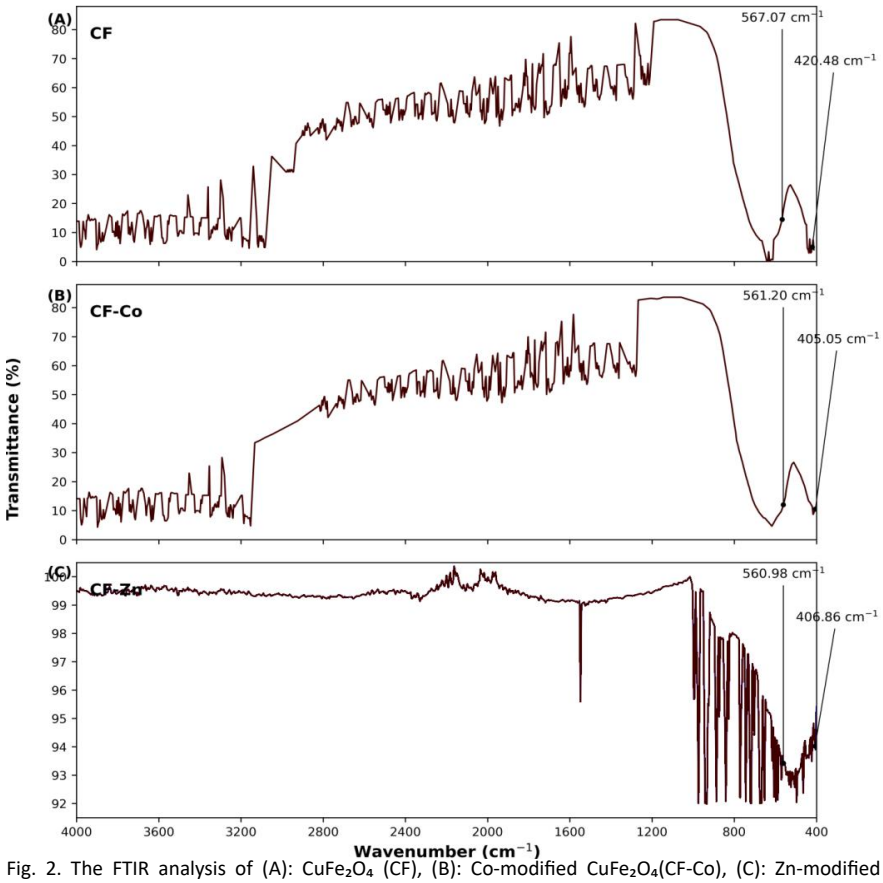


Fig. 2. The FTIR analysis of (A): $CuFe_2O_4$ (CF), (B): Co-modified $CuFe_2O_4$(CF-Co), (C): Zn-modified $CuFe_2O_4$(CF-Zn) powders annealing at 800°C .

Table 1. The FTIR analysis of (A): $CuFe_2O_4$ (CF), (B): Co-modified $CuFe_2O_4$(CF-Co), (C): Zn-modified $CuFe_2O_4$(CF-Zn) powders annealing at 800 ℃.

Sample	Tetrahedral band (v_1) (A-site) cm^{-1}	Octahedral band (v_2) (B-site) cm^{-1}
CF	567.07	420.48
CF-Co	561.20	405.05
CF-Zn	560.98	406.86

CC BY

24 h, and later three serial dilutions occur, and 100 µl of the last dilution is cultured in Mueller-Hinton Agar (MHA) for 24 h at 37°C, and the survival percentage is calculated according to Eq. 1 to determine the killing percentage [16]:

$$\text{Survival \%} = \frac{\text{number of Colony bacterial treated}}{\text{number of Colony control bacteria}} \text{x } 100 \quad (1)$$

Eq. 2 was initially used to get the survival %. The following relationship was then used to get the antibacterial killing percentage:

$$\text{Killing (\%)} = 100 - \text{Survival (\%)} \quad (2)$$

To prevent microbial contamination, all produced nanoparticle powders were sterilized before the antibacterial tests. An untreated bacterial culture served as the negative control in all antibacterial tests, which were carried out in triplicate (n = 3)., the mean ± standard deviation (SD) is used to express the results of all antibacterial studies. Since the aim of the current study was to evaluate the antibacterial activity of the synthesized Nano materials with the untreated control under identical experimental conditions, a standard antibiotic was excluded as a positive control. The mean ± standard deviation (SD) is used to express the results of all antibacterial studies, which were conducted in triplicate (n = 3).

RESULTS AND DISCUSSION

Fourier transforms infra-red spectroscopy FTIR analysis

FTIR analysis confirmed the formation of the spinel ferrite structure and provided evidence of cation distribution in the synthesized samples of both pure $CuFe_2O_4$ ferrite and ferrite modified by Co and Zn, as seen in Fig. 2 and Table 1, which show two absorption bands between 400 and 600 cm^{-1} that depend on composition and correspond to the octahedral and tetrahedral sites of the positive ions, respectively, and are associated with the tetrahedral site. It is discovered that band locations [14, 17, 18].

For original $CuFe_2O_4$ (CF), the distinctive metal–oxygen vibration band was found at 567.07 cm^{-1}; for Co-modified $CuFe_2O_4$ (CF-Co) and Zn-modified $CuFe_2O_4$ (CF-Zn), it shifted to 561.20 cm^{-1} and 560.98 cm^{-1}, respectively. As a result, the addition of Co^{2+} and Zn^{2+} caused downward movements of roughly 5.87 and 6.09 cm^{-1}, respectively. These changes show that the cation distribution and local metal-oxygen bonding environment within the spinel lattice have changed. Changes in the identity and distribution of cations between tetrahedral (A) and octahedral (B) sites in Zn-modified / Co-modified $CuFe_2O_4$ can influence the force constants, which in turn can change the characteristic metal–oxygen vibrational frequencies [19-21] revealed composition-dependent structural behavior for Co-containing spinel ferrites, which is in line with the observed shift. Furthermore, the octahedral-associated band moved by around 15.43 and 13.62 cm^{-1}, respectively, from 420.48 cm^{-1} in CF to 405.05 cm^{-1} in CF-Co and 406.86 cm^{-1} in CF-Zn. These modifications also show that the local cation-oxygen habitats have changed after being modified with Co^{2+} and Zn^{2+}. Following Zn and Co alteration, changes in the local metal–oxygen bonding environment and the structural properties of the $CuFe_2O_4$ ferrite are shown by the systematic shifts in the characteristic FTIR bands and the observed changes in the XRD structural parameters. However, FTIR cannot conclusively determine the particular crystallographic site occupancy or chemical composition of Zn^{2+} and Co^{2+}. [19-21].

Fe^{3+} ions move to the octahedral sites, reducing the tetrahedral vibration frequency, while Zn^{2+} and Co^{2+} ions are introduced to the tetrahedral sites with bigger radii and greater atomic weight. Similarly, the octahedral vibration band shifted toward lower wavenumbers, indicating a decrease in the octahedral vibration frequency. [20]. As a result, for samples modified with Co and Zn, the absorption band moved from 567.07 cm^{-1} to lower values of 561 and 560 cm^{-1}, respectively. These results are consistent with earlier reports on doped spinel ferrites [19-21], which observed shifts in the metal-oxygen bond vibration bands—associated with tetrahedral and octahedral sites—indicate changes in the local bonding environment following modification with zinc (Zn) and cobalt (Co), may be attributed to variations in cation distribution and local lattice interactions within the spinel structure. However, Fourier-transform infrared (FTIR) spectroscopy alone cannot be relied upon to determine precise crystallographic sites or to definitively confirm the specific locations of Zn^{2+} and Co^{2+} ions. Consequently, the observed spectral shifts serve as supporting evidence for structural modification, rather than conclusive proof that the cations occupy specific, well-defined sites.

CC BY

XRD analysis

The produced CF, CF-Zn, and CF-Co ferrites' XRD patterns showed the distinctive reflections of a cubic spinel ferrite structure. The primary diffraction peaks are seen at roughly 18.3°, 30.1°, 35.5–35.9°, 43.3°, 57.2°, and 62.8°, which correspond to the (111), (220), (311), (400), (511), and (440) planes, respectively. These values are broadly comparable with the standard JCPDS card No. 34-0425 for $CuFe_2O_4$. The Debye-Scherrer equation was used to determine the crystallite size of the most intense (311) reflection. The (311) reflection's 2θ location was roughly 35.9°, 35.7°, and 35.6° for CF, CF-Zn, and CF-Co, respectively, as shown in Table 2. The average crystallite sizes were 11.7, 20.8, and 17.3 nm, respectively, based on the corresponding FWHM values of around 0.714°, 0.401°, and 0.482°. The greater estimated crystallite sizes in comparison to the unmodified CF sample are thus linked to the shorter (311) peak widths seen for the Zn- and Co-modified samples. These findings suggest that the crystal-growth behavior during the annealing process is influenced by the addition of Zn and Co [22, 23].

It is not necessary to automatically interpret weak reflections seen at higher diffraction angles—such as those close to 37.5°, 53.5°, and 74–75°—as proof of a distinct dominant crystalline phase. These weak characteristics, especially in the areas around 38–39° and 53–54°, can result from higher-order reflections of the spinel structure and may also overlap with reflections linked to small CuO-related phases. The XRD results are therefore interpreted as showing a predominantly spinel $CuFe_2O_4$ structure with no clearly resolved dominant secondary crystalline phase within the detection capability of the measurement, taking into account the relative intensity of these features and the overall agreement of the major reflections with the $CuFe_2O_4$ spinel pattern.

As one moves from the unmodified $CuFe_2O_4$ (CF) sample to the samples containing zinc (Zn) and cobalt (Co), the computed lattice parameter values increase. In particular, the lattice parameter increased from 8.28 Å for the CF sample to 8.34 Å for the CF-Zn sample and 8.36 Å for the CF-Co sample. Changes in the local structural environment, lattice deformation, or possible cation redistribution during the synthesis and heat treatment (annealing) procedures could all be responsible for this rise. Cation redistribution between the tetrahedral (A) and octahedral (B) sites, local lattice distortion, and residual strain produced during synthesis and annealing can all have an impact on the change in lattice parameter in addition to the ionic radius of the inserted cation. Therefore, structural modification after Zn and Co insertion is supported by the observed changes in lattice parameter and crystallite size as well as the systematic shifts of the FTIR metal–oxygen bands. Thus, the XRD results show that the $CuFe_2O_4$ ferrite system's crystallographic dimensions and crystal-growth characteristics are affected by the compositional alteration. However, these structural alterations cannot be solely attributed to the incorporation of Zn^{2+} or Co^{2+} ions into particular crystallographic sites because the elemental composition and the distribution of cations throughout the crystallographic sites were not explicitly determined.

The Bragg angle of the chosen peak is equal to the diffraction angle (θ). As a result, the average crystalline sizes, as seen in Table 2, were calculated from the peak (311) of the XRD diffractogram, employing Scherrer's formula [24] calculated by Eq. 3, where the practical size found increased when Zn and Co were found:

$$D = \frac{0.9 * \lambda}{\beta \cos\theta} \quad (3)$$

The X-ray density and lattice constant were calculated using conventional XRD data. Eq. 3 was used to compute the lattice constant, which was found using the Nelson Riley extrapolation method [25]. The lattice constant was found to increase when Zn and Co are found by:

Bragg's law (nλ=2d sinθ), where (n=1) is the diffraction order, (λ =1.5406) Å is the wavelength of Cu Kα radiation, and (θ) is the Bragg angle corresponding to half of the measured (2θ) value, was used to calculate the interplanar spacing (d) from the measured diffraction angle, as a result, (λ=2d sinθ) and (d) was computed using (d= λ/2sinθ). The lattice parameter of the cubic spinel structure was then determined using the obtained interplanar spacing in Eq. 4, where (h), (k), and (l) stand for the Miller indices of the appropriate diffraction plane.

$$\alpha^2 = (h^2 + k^2 + l^2) * d^2 \quad (4)$$

d is the interplanar spacing, and h, k, and l are the miller index.

CC BY

Where x-ray density was increasing when Zn ions and Co ions are found, which was calculated by Eq. 5

$$\rho x = \frac{8 * Mw}{NA * a^3} \quad (5)$$

MW=molecular Wight, Na= Avogadro's number, a=lattice constant

The X-ray density of the samples was estimated by Eq. 5, based on the assumption that there are eight formula units in each unit cell (Z = 8) of the cubic spinel structure. The molecular weight of $CuFe_2O_4$ (239.232 g/mol), and the revised lattice parameter (8.28 Å) were utilized for the calculation of the theoretical X-ray density of the unmodified $CuFe_2O_4$ (CF) sample, which gave a value of about 5.61 g/cm³.

Changes in the average crystal structure, localized lattice distortion, or maybe a redistribution of metal cations during synthesis and heat treatment could be the cause of the significant rise in the crystal lattice constant for samples containing zinc and cobalt. Zinc (Zn^{2+}) and cobalt (Co^{2+}) ions' individual contributions to this alteration cannot be isolated, despite the fact that ionic size can affect the lattice dimensions of spinel ferrites. Consequently, rather of being a direct

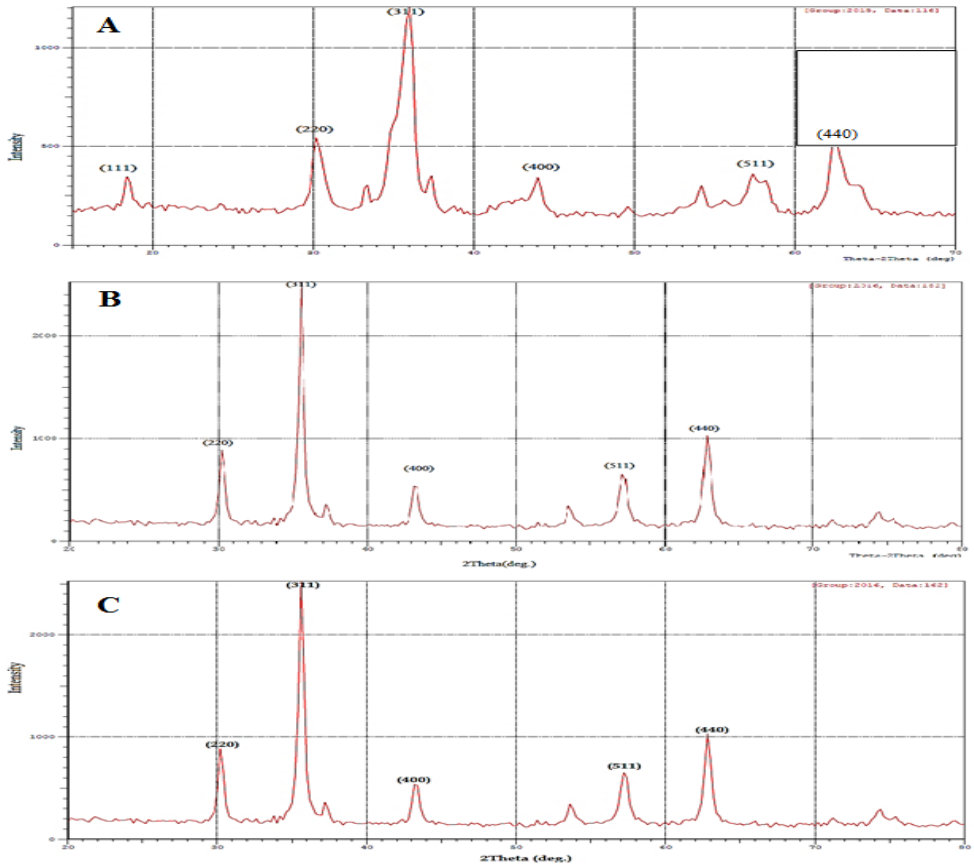


Fig. 3. The XRD analysis of (A): $CuFe_2O_4$ (CF), (B): Co-modified $CuFe_2O_4$(CF-Co), (C): Zn-modified $CuFe_2O_4$(CF-Zn) powders annealing at 800°C .

Table 2. presents the XRD parameters of the synthesized samples.

Samples	Lattice Constant a (Å)	x-ray density ρ_x (g/cm³)	crystalline sizes (nm)	FWHM (311) (°)	2θ (311) (°)
CF	8.28	5.61	11.7	0.71	35.9
CF-Zn	8.34	-	20.8	0.401	35.7
CF-Co	8.36	-	17.3	0.482	35.6

CC BY

confirmation of the structural alterations in the prepared samples, the observed variations in the crystal lattice constant are taken as an indication of structural changes within the prepared samples. Previous research has demonstrated similar behavior for modified $CuFe_2O_4$ spinel ferrites [26, 27].

SEM analysis

The SEM images of (A): $CuFe_2O_4$ (CF), (B): Co-modified $CuFe_2O_4$ (CF-Co), and (C): Zn-modified $CuFe_2O_4$ (CF-Zn) powders that were annealed at 800 °C are displayed in Fig. 4. All samples exhibit visible pores and agglomerated particles with irregular morphology. Ferrite nanoparticles' high surface energy and magnetic interactions, which encourage particle clustering during synthesis, are responsible for the agglomeration behavior. Furthermore, annealing at 800 °C encourages particle growth and partial fusion between nearby particles, producing rough surface features and compact aggregates [27].

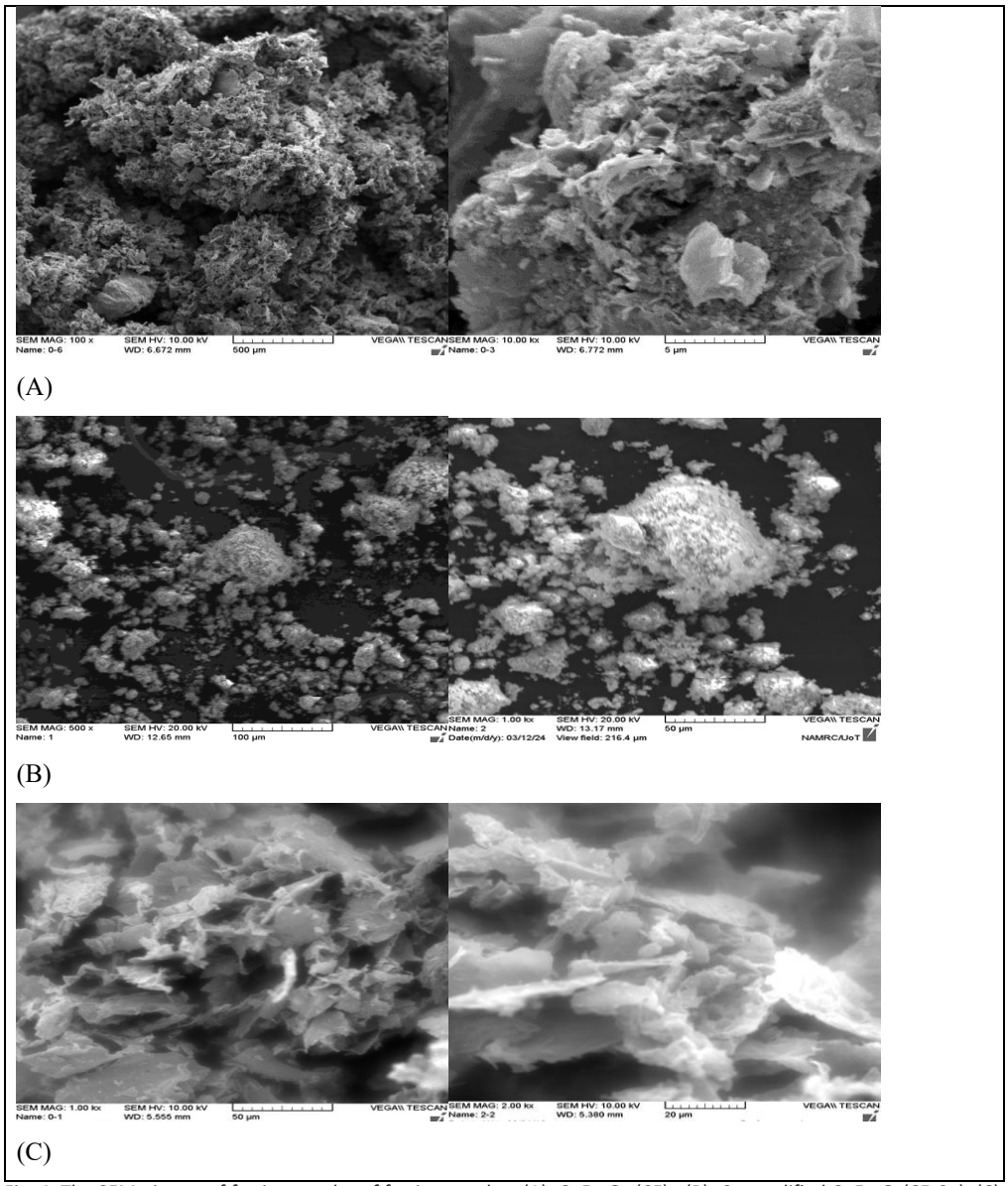


Fig. 4. The SEM picture of ferrite powder of ferrite powders (A): $CuFe_2O_4$ (CF) , (B): Co-modified $CuFe_2O_4$(CF-Co), (C): Zn-modified $CuFe_2O_4$(CF-Zn) powders annealing at 800°C .

(cc) BY

Due to altered crystal growth behavior and lattice distortion, the addition of Zn^{2+} and Co^{2+} ions further altered the particle shape, resulting in more irregular and porous architectures. The effective surface area and interaction between the ferrite particles and bacterial cells may be increased by such rough and porous morphologies. For spinel ferrites made via co-precipitation and subsequent heat treatment, comparable morphological characteristics have been documented.

The surface morphology of the synthetic ferrite samples can be qualitatively compared using the SEM images. The high surface energy of the small particles and the heat treatment used during synthesis may be responsible for the particles' erratic morphology and propensity for agglomeration. The examined compositions differ in terms of surface roughness and the degree of aggregation. However, rather from being utilized to precisely determine the size of individual particles, the SEM data are interpreted qualitatively because the available SEM pictures

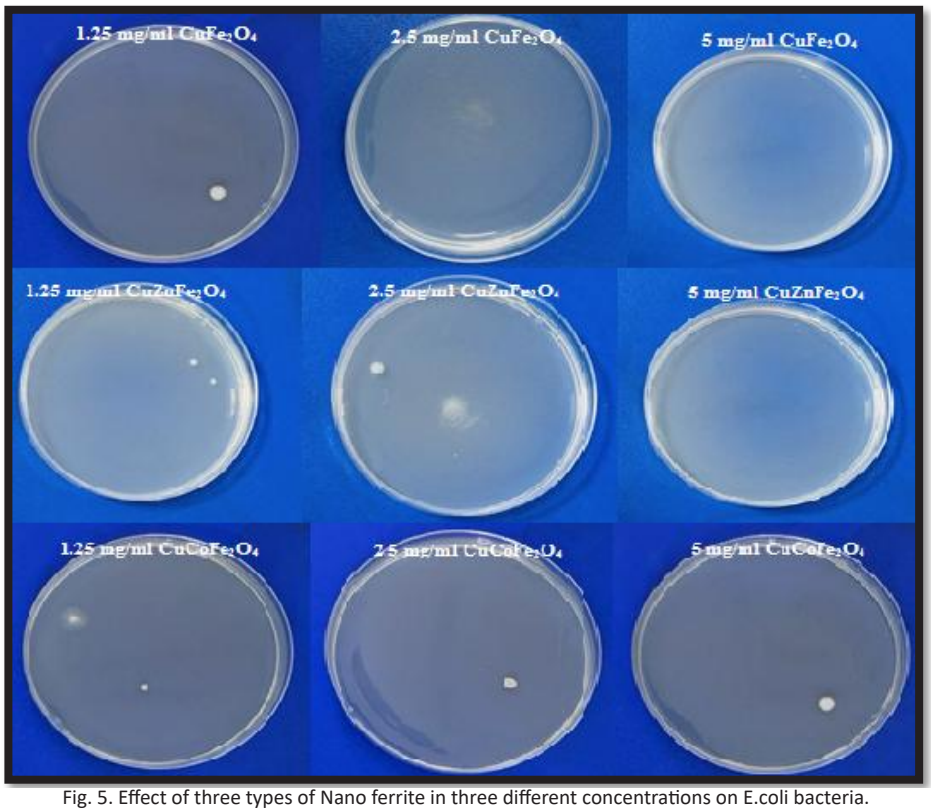


Fig. 5. Effect of three types of Nano ferrite in three different concentrations on E.coli bacteria.

Table 3. Percentage killing (%) of Nano ferrite

Materials	concentration	percentage of killing %	
		Ecoli	Staph.aureus
		Mean±SD	Mean±SD
CF	1.25 mg/ml	99 ±1.4	84±4.3
	2.5mg/ml	99.4±0.8	90±2.1
	5 mg/ml	100±0.0	95±1.4
CF-Zn	1.25mg/ml	96±2.2	77±1.6
	2.5mg/ml	97±1.22	85±3.7
	5mg/ml	100±0.00	90±2.1
CF-Co	1.25mg/ml	97±2.4	96±2.1
	2.5mg/ml	97±1.08	97±0.8
	5 mg/ml	98±0.4	99±*1.70*

CC BY

were obtained at varying magnifications and higher-magnification images were not accessible. As a result, the structural data from XRD and FTIR should be complemented by the observed morphological traits.

Results and discussion of antibacterial

Overall, the produced ferrite nanoparticles showed potent antibacterial activity against both Gram-positive S. aureus and Gram-negative E. coli. The Co-modified $CuFe_2O_4$ sample likewise showed good antibacterial performance against S. aureus, attaining inhibition values of up to 99%, even though several samples showed slightly higher antibacterial activity against E. coli. As a result, rather than depending just on the Gram classification, the antibacterial activity was dependent on both the bacterial strain and the composition of the nanoparticles.

The results demonstrated ability of several Nano ferrite materials to effect on both types of bacteria (Table 3), which is consistent with [5] with serial concentrations (1.25, 2.5, 5) mg/ml , where the percentage of killing E.Coli bacteria was (99, 99.4,

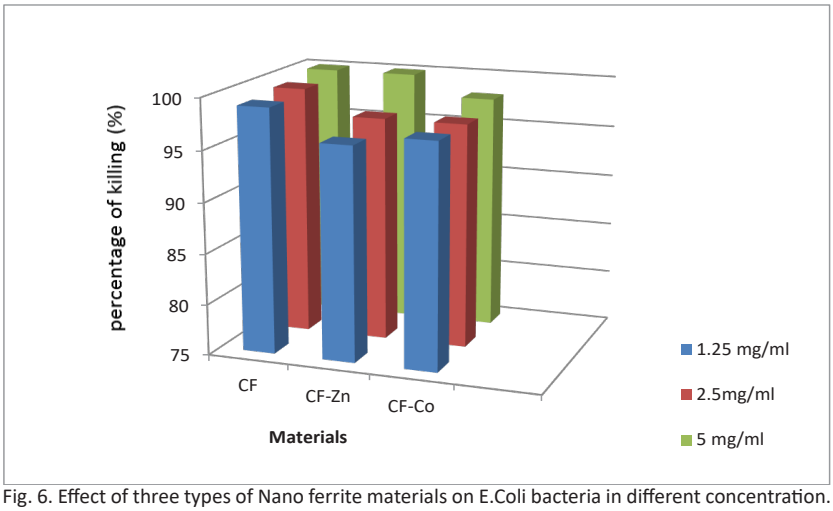


Fig. 6. Effect of three types of Nano ferrite materials on E.Coli bacteria in different concentration.

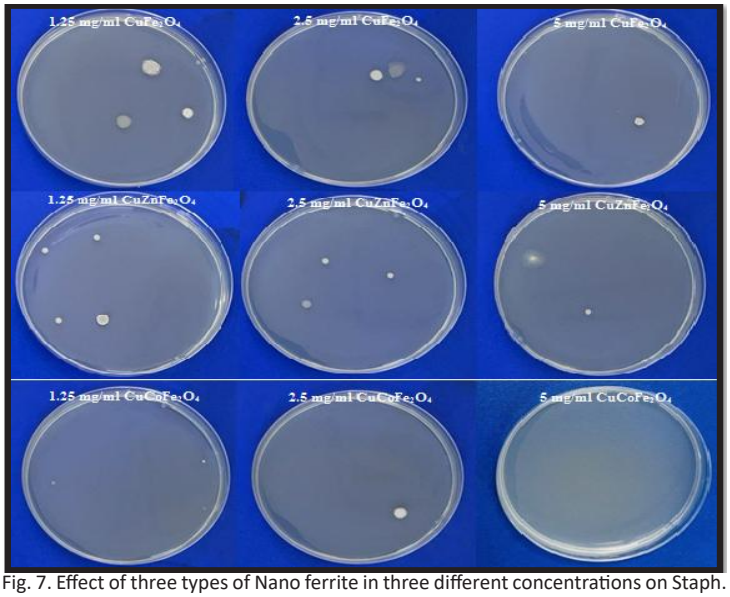


Fig. 7. Effect of three types of Nano ferrite in three different concentrations on Staph. aureus bacteria.

CC BY

100)%, (96, 97, 100)%, and (97, 97, 98)% when used $CuFe_2O_4$ (CF) ,Zn-modified $CuFe_2O_4$(CF-Zn) and Co-modified $CuFe_2O_4$(CF-Co) respectively as seen in Figs. 5 and 6, Also, the killing percentage of Staphylococcus aureus was (84, 90, 95) % ,(77, 85, 90) % and (96,97,99) % when used $CuFe_2O_4$ (CF) ,Zn-modified $CuFe_2O_4$(CF-Zn) and Co-modified $CuFe_2O_4$(CF-Co), respectively in the same serial concentration as seen in Figs. 7 and 8.

The matching mean and SD for samples exhibiting 100% bacterial death in all three replicates were reported as 100 ± 0.00%, suggesting that no bacterial colonies were found in the plated samples under the experimental circumstances.

The produced ferrite-based materials' demonstrated antibacterial activity is in line with other research that found metal-containing ferrite nanoparticles to have antibacterial qualities [5, 28]. Additionally, potential interactions between metal ions and bacterial cell components have been linked to the antibacterial activity of products containing copper [13]. Cu ions' antibacterial activity may be attributed to membrane disruption and increase permeability of the cytoplasmic membrane by interaction of ions with phosphorus and sulfur in DNA, and according to previous studies, it may inhibit protein synthesis by destruction of cytoplasmic ribosomes [29]. Nevertheless, no direct investigation was conducted into the precise mechanisms behind the antibacterial activity seen in the current samples.

Variations in the content and structural characteristics of the produced ferrite samples may be responsible for the observed discrepancies in antibacterial activity. According to earlier research, bacterial cells can be impacted by metal-containing nanomaterials through a variety of interactions, such as ion-related impacts and cell membrane rupture [29]. However, this study did not specifically look at the mechanisms underlying the produced samples' antibacterial activity.

$CuFe_2O_4$ ferrites' crystallite size, lattice parameter, and FTIR band locations were all altered by Zn and Co inclusion, according to structural characterization. Variations in antibacterial activity coincided with these structural alterations, indicating a relationship between the ferrite nanoparticles' biological performance and their structural features.

The lack of a typical antibiotic positive control is one of the current antibacterial study's limitations. The absence of a reference antibiotic makes it difficult to compare the antibacterial efficacy of the synthesized ferrites with traditional antimicrobial drugs, even if an untreated bacterial culture was used as a negative control to establish baseline bacterial growth. However, the three ferrite-based materials could be compared under the same testing conditions thanks to the experimental

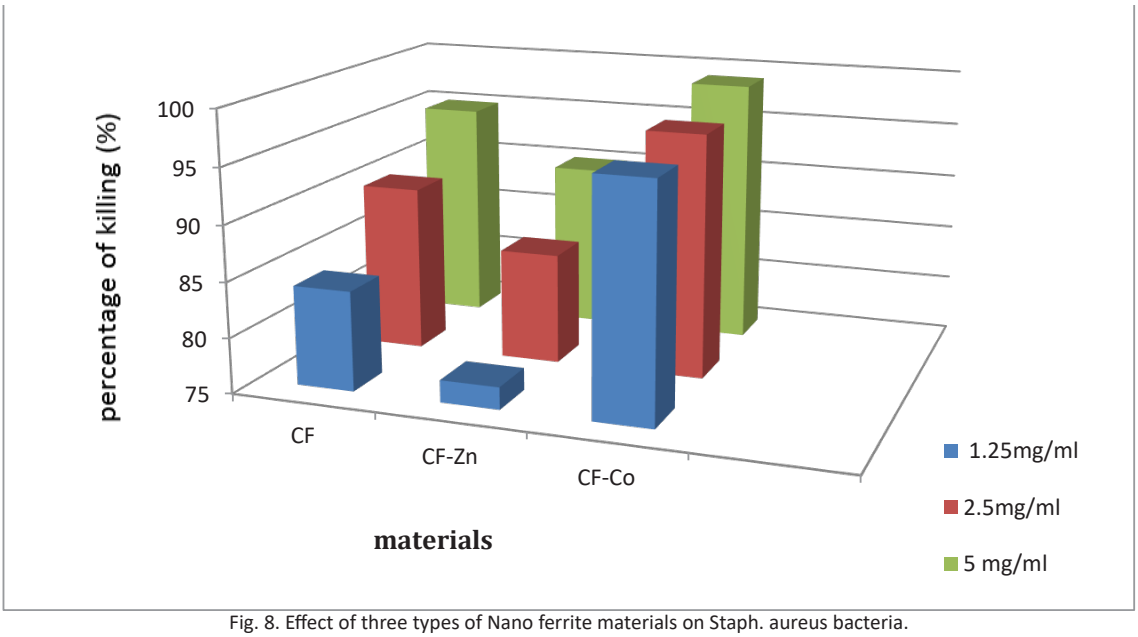


Fig. 8. Effect of three types of Nano ferrite materials on Staph. aureus bacteria.

design.

Correlation between structural characteristics and antibacterial efficacy

The comparative research shows that the structural properties of the produced ferrites are directly linked to their antibacterial activity. For all samples, XRD analysis verified the creation of a predominantly spinel structure; however, following Zn and Co incorporation, minor changes in crystallite size and lattice parameter were noted. The tetrahedral and octahedral metal–oxygen vibration bands in the FTIR spectra also displayed slight shifts, indicating modifications in the distribution of cations inside the spinel lattice. Among the produced ferrites, SEM studies showed aggregated particles with various surface morphologies. It is anticipated that these structural changes will affect the surface properties and the way the ferrite particles interact with bacterial cells. Therefore, rather than a single structural parameter, the variations in antibacterial activity among the synthesized samples can be attributable to the combined influence of their surface morphology, cation distribution, crystallite size, and crystal structure.

CONCLUSION

$CuFe_2O_4$ nanoferrite and two other ferrite-based samples made with Zn^{2+} and Co^{2+} precursor additions were produced using the co-precipitation method and then annealed at 800 °C. They were compared in terms of their morphological, structural, and antibacterial characteristics. which were examined the structural, morphological, and antibacterial properties of them. The distinctive metal–oxygen vibrations connected to the spinel ferrite structure's tetrahedral and octahedral sites were validated by the FTIR data. Following Zn and Co modification, systematic shifts in the characteristic bands are compatible with structural modification of the $CuFe_2O_4$ lattice and show alterations in the local metal–oxygen bonding environment. The XRD data revealed the distinctive diffraction reflections of a spinel ferrite structure that is mostly cubic. The (311) reflection was utilized to estimate crystallite size, and the primary reflections were attributed to the relevant crystallographic planes of the spinel structure. For CF, CF-Zn, and CF-Co, the computed crystallite sizes were 11.7 nm, 20.8 nm, and 17.3 nm, respectively. The average structural properties of the produced materials changed when the lattice parameter increased from 8.28 Å for CF to 8.34 Å for CF-Zn and 8.36 Å for CF-Co. However, more elemental analysis is needed to determine the precise cation-site occupancy and chemical makeup of the Zn and Co-containing samples. These differences show that the ferrite system's structural characteristics and crystal-growth behavior were impacted by Zn and Co alteration. SEM observations showed varying degrees of aggregation along with irregular particle morphologies. These characteristics are in line with the thermal treatment used during preparation and the fine particle nature of the synthesized ferrites. Rather than being used to precisely determine the size of individual particles, the morphological observations were interpreted qualitatively because the available SEM pictures were collected at varied magnifications.

All ferrite samples under investigation showed significant bacterial death in the antibacterial tests against Staphylococcus aureus and Escherichia coli. CF and CF-Zn killed 100% , while CF-Co killed 98% of E. coli at 5 mg/mL. The killing percentages for S. aureus rose with concentration, reaching 95% for CF, 90% for CF-Zn, and 99% for CF-Co at 5 mg/mL. These results show that, under the evaluated experimental conditions, the synthesized ferrites exhibit strong concentration-dependent antibacterial activity, which cannot be exclusively attributable to the bacterial strain's Gram classification, Since the molecular mechanism causing bacterial death is not directly identified in this study, potential contributions from surface interactions, ion-related effects, oxidative processes, or other mechanisms should be considered literature-supported possibilities rather than experimentally confirmed mechanisms in this work.

ACKNOWLEDGEMENT

The authors would like to extend my thanks and gratitude to all those who contributed to this scientific research, especially the staff of the Nanotechnology and Advanced Materials Research Center / University of Technology / Baghdad / Iraq, hoping that this study would benefit all facets of humanity.

CONFLICT OF INTEREST

The authors declare that there is no conflict of interests regarding the publication of this manuscript.

CC BY

REFERENCES

1. Parajuli D, Murali N, Samatha K. Cr3+ substitution effect on Co-Cu and Cu-Co nano ferrites on structural and morphological properties. BIBECHANA. 2023;20(3):275-284.
2. Rao A, Thakur P, Thakur A. Future Perspectives of Spinel Nano-Ferrites. Applications of Spinel Nano-Ferrites in Health, Environmental Sustainability, and Safety: CRC Press; 2025. p. 213-224.
3. Structural, dielectric and ac electrical properties of nano-structured $Mn_{0.6}Co_{0.2}Ni_{0.2}Fe_2O_4$ ternary ferrite synthesized by citrate-gel auto-combustion technique. Indian Journal of Pure and Applied Physics. 2022.
4. Andhare DD, Jadhav SA, Khedkar MV, Somvanshi SB, More SD, Jadhav KM. Structural and Chemical Properties of ZnFe2O4 Nanoparticles Synthesised by Chemical Co-Precipitation Technique. Journal of Physics: Conference Series. 2020;1644(1):012014.
5. Jaid GM, Bohan AJ, Salman GK. Artificial Neural Network Modeling for Removal of Cd (II) and Pb (II) from Wastewater by Using Three Ferrite Nanomaterial ($Cu_{0.9}Zn_{0.1}Fe_2O_4$, $Cu_{0.8}Zn_{0.2}Fe_2O_4$, and $Cu_{0.7}Zn_{0.3}Fe_2O_4$) and Study the Antimicrobial Effectiveness of these Ferrite Substances. Rev Chim. 2020;71(10):67-80.
6. Rawdhan RR, Salman GK, Ismail MM. Mechanical and durability properties of cementitious brick containing Nano Ferrite. IOP Conference Series: Materials Science and Engineering. 2020;737(1):012076.
7. Dhiman M, Chudasama B, Kumar V, Tikoo KB, Singhal S. Augmenting the photocatalytic performance of cobalt ferrite via change in structural and optical properties with the introduction of different rare earth metal ions. Ceram Int. 2019;45(3):3698-3709.
8. Mulud FH, Dahham NA, Waheed IF. Synthesis and Characterization of Copper Ferrite Nanoparticles. IOP Conference Series: Materials Science and Engineering. 2020;928(7):072125.
9. Jain R, Kumar S, Meena SK. Precipitating agent (NaOH and NH4OH) dependent magnetic properties of cobalt ferrite nanoparticles. AIP Advances. 2022;12(9).
10. Kumar P, Channi HK. Spinel and Inverse Ferrites for Drug Delivery. Spinel and Inverse Spinel Ferrites: Chapman and Hall/CRC; 2025. p. 70-88.
11. Biswas K, R K, Inbathamizh L, Islam NF, Sarma H. Spinel ferrite nanoparticles: Multifaceted applications and future perspectives in biomedical and environmental sciences. Next Research. 2026;5:101364.
12. Chawngthu Z, Singh TA, Sadhukhan P, Kumar D, Das J. A comprehensive review on the plant-mediated synthesis of green nanoferrites for anticancer, antibacterial, antioxidant, sensing and photocatalytic wastewater treatment applications. Materials Today Chemistry. 2026;53:103576.
13. Lemire JA, Harrison JJ, Turner RJ. Antimicrobial activity of metals: mechanisms, molecular targets and applications. Nature Reviews Microbiology. 2013;11(6):371-384.
14. Hutamaningtyas E, Utari, Suharyana, Wijayanta AT, Purnama B. FTIR and structural properties of co-precipitated cobalt ferrite nano particles. Journal of Physics: Conference Series. 2016;776:012023.
15. Azhar JB, Ghaed KS, Duha SA. Enhanced bioactivity of Pure ZnO and ZnO-Ag nanocomposite Using Sol-Gel method for Self-Cleaning Application. International Journal of Research in Pharmaceutical Sciences. 2019;10(4):3649-3656.
16. Jabbar Bohan A, Khalef Salman G, Majeed Jaid G. Comparative Study between Zn and Cu Nano Ferrite in Removal of Heavy Metals and Microorganisms from Water. Diyala Journal For Pure Science. 2021;17(4):1-19.
17. Vijaya Bharathi R, Raju MK, Uppugalla S, Raghavendra V, Parajuli D, Suryanarayana B, et al. Cu^{2+} substituted Mg-Co ferrite has improved dc electrical resistivity and magnetic properties. Inorg Chem Commun. 2023;149:110452.
18. Baburao B, Hari Kumar N, Edukondalu A, Venkata Narayana M, Ravinder D. Structural, optical, DC electrical, thermo-electric, dielectric and magnetic properties of $Mg_{0.8}Zn_{0.2}Gd_xFe_{2-x}O_4$ nanoparticles synthesised by citrate-gel auto combustion method. Inorg Chem Commun. 2023;148:110355.
19. Belavi PB, Chavan GN, Naik LR, Somashekar R, Kotnala RK. Structural, electrical and magnetic properties of cadmium substituted nickel–copper ferrites. Materials Chemistry and Physics. 2012;132(1):138-144.
20. Nakamura T. Snoek's limit in high-frequency permeability of polycrystalline Ni–Zn, Mg–Zn, and Ni–Zn–Cu spinel ferrites. J Appl Phys. 2000;88(1):348-353.
21. Sherstyuk DP, Zhivulin VE, Starikov AY, Pesin LA, Sozykin SA, Gudkova SA, et al. CORRELATION BETWEEN CHEMICAL COMPOSITION AND CURIE TEMPERATURE OF A NICKEL-COBALT FERRITE. J Struct Chem. 2023;64(9):1743-1750.
22. Ramakrishna A, Murali N, Margarette SJ, Samatha K, Veeraiah V. Comparative study of synthesis, structural and magnetic properties of Cu^{2+} substituted Co-Ni, Co-Zn and Co-Mg nano ferrites. Physica B: Condensed Matter. 2018;530:251-257.
23. Rajasekhar Babu K, Purnachandra Rao M, Subba Rao PSV, Rama Rao K, Kishore Babu B, Rajesh Babu B. Structural and Magnetic Properties of Cu^{2+} Substituted Co–Zn Ferrite Nanoparticles, Synthesized by Sol–Gel Combustion Method. Journal of Inorganic and Organometallic Polymers and Materials. 2017;27(3):612-621.
24. Kadam RH, Borade RB, Mane ML, Mane DR, Batoo KM, Shirsath SE. Structural, mechanical, dielectric properties and magnetic interactions in Dy^{3+} -substituted Co–Cu–Zn nanoferrites. RSC Advances. 2020;10(47):27911-27922.
25. Qamar S, Akhtar MN, Batoo KM, Raslan EH. RETRACTED: Structural and magnetic features of Ce doped Co-Cu-Zn spinel nanoferrites prepared using sol gel self-ignition method. Ceram Int. 2020;46(10):14481-14487.
26. Parajuli D, Murali N, Rao AV, Ramakrishna A, S YM, Samatha K. Structural, dc electrical resistivity and magnetic investigation of Mg, Ni, and Zn substituted Co-Cu nano spinel ferrites. South African Journal of Chemical Engineering. 2022;42:106-114.
27. Akhtar MN, Alelyani M, Babar M, Baqir MA, Siddique MA, Irfan M, et al. Magnetodielectric, elastic, Rietveld refinement and absorption properties of Nd–Cu co-doped Co–Zn nano ferrites: Development of meta-absorbers for wide frequency regime. Ceram Int. 2024;50(8):12890-12904.
28. Velayutham L, Parvathiraja C, Anitha DC, Mahalakshmi K, Jenila M, Alasmary FA, et al. Photocatalytic and Antibacterial Activity of CoFe2O4 Nanoparticles from Hibiscus rosa-sinensis Plant Extract. Nanomaterials. 2022;12(20):3668.
29. Yin IX, Zhang J, Zhao IS, Mei ML, Li Q, Chu CH. The Antibacterial Mechanism of Silver Nanoparticles and Its Application in Dentistry. International Journal of Nanomedicine. 2020;Volume 15:2555-2562.

CC BY